Evaluation of Direct Signal Suppression for Passive Radar

Joseph Landon Garry, *Member, IEEE*, Chris J. Baker, *Fellow, IEEE*, and Graeme E. Smith, *Senior Member, IEEE*

***Abstract*— Passive radar (PR) systems must be able to detect the presence of a target signal many orders of magnitude weaker than the direct signal interference (DSI). Due to the continuous nature of most PR signals, this interference, rather than thermal noise, determines the sensitivity of the system. Suppression of DSI and clutter prior to range-Doppler processing is crucial for maximizing the effective dynamic range, to increase detection range and improve overall system performance. A number of time-domain adaptive filtering techniques have been proposed to mitigate the effects of DSI, with varying levels of success. As such, an investigation of the primary factors affecting suppression performance is presented, using Advanced Television Systems Committee digital television (DTV) waveforms as an example, through simulation and extensive experimental trials. A number of spectral and spatially diverse DTV signals are considered to analyze suppression performance under a wide range of realistic scenarios. In particular, the fast block least mean squares filter is shown to provide good suppression performance with low computational requirements. Results of this analysis can be used to predict PR performance and stability. Practical metrics, such as suppression runtime and ease of implementation, also serve to counsel selection of DSI mitigation algorithms for experimental systems.**

***Index Terms*— Adaptive filters, interference suppression, radar, radar signal processing.**

I. Introduction

PASSIVE radar (PR) systems, which utilize illuminators of opportunity rather than a dedicated transmitter, offer a number of distinct advantages compared with traditional active radar systems. The use of opportunistic transmissions results in a system which imposes no additional spectral requirements in an increasingly congested electromagnetic environment. The absence of transmitter hardware is potentially more cost efficient and utilizes significantly less power than active radars. This also results in an inherently stealthy system with a low probability of intercept, great advantages for military situations. Despite the numerous advantages, the bistatic geometries and continuous wave transmissions of most broadcast illuminators add significant complexity and necessitate additional processing stages to exploit these benefits. Chief among these processes is suppression of the direct signal interference (DSI) term, which if not compensated for can severely cripple the sensitivity of a PR.

Manuscript received June 20, 2016; revised October 29, 2016; accepted February 27, 2017. Date of publication April 4, 2017; date of current version June 22, 2017.

J. L. Garry and G. E. Smith are with the Electrical and Computer Engineering Department, The Ohio State University, OH 43210-2500 USA (e-mail: garry.6@osu.edu).

C. J. Baker is with Aveillant, Radar Systems, Cambridge CB4 0XL, U.K.

Digital Object Identifier 10.1109/TGRS.2017.2680321

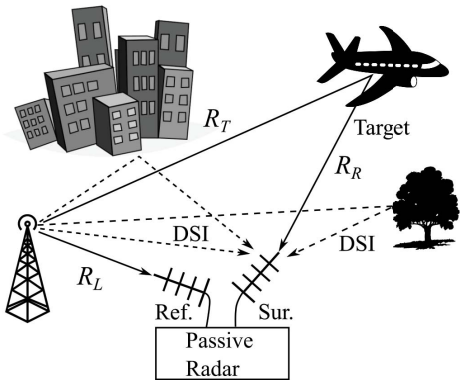

Fig. 1. Illustration of PR DSI scenario.

A typical PR receiver consists of two primary channels, the surveillance and reference channel. The surveillance channel serves to record the signals scattered from any targets within the beam pattern of the surveillance antenna, as shown in Fig. 1. The reference channel gathers a time-delayed replica of the transmitted signal, which can be processed against the surveillance waveform to create a 2-D surface indicating range and velocity. In practice, this idealized model is far from reality. The surveillance channel also contains direct signal leakage, multipath, and strong ground clutter reflections, all of which comprise the DSI [1]. The effective noise floor of the range-Doppler (RD) map is set by this level, as will be demonstrated in Sections II–IV. Analog methods of suppressing this interference, such as antenna null-steering, physical shielding, and hardware cancellation are moderately effective but ultimately limit system flexibility. To utilize multiple illuminators and various bistatic geometries, and arguably primary advantages of PR systems, digital methods of adaptive filtering are necessary.

This paper serves to predict the performance and benchmark of a number of time-domain DSI mitigation techniques, along with providing an extensive overview of factors affecting suppression performance. Both classical adaptive filtering methods [2] and more recent algorithmic developments in DSI suppression [3], [4] will be evaluated using extensive theoretical and experimental verification. These include suppression performance in terms of mean, variance over time, RD clutter null width, and runtime, along with additional remarks on the implementation considerations. All predominant factors that affect suppression performance will be discussed, which include signal purity, PR processing effects, and the DSI suppression algorithms and related parameters.

Signal purity involves the presence of noise, interference, and clutter in both channels of a given PR system, while the PR processing primarily concerns the choice of coherent processing interval. All of these parameters vary widely between various PR instantiations, which, in turn, potentially requires adjustments in the choice of suppression algorithm and its tunable parameters to deal with changing scenarios and operation goals.

The power-related equations for modeling the signal levels, DSI suppression, and the effects of the PR processing will also be developed, such that a system's effective noise level can be calculated. This value is one of the fundamental parameters, which directly influences almost every radar operation. Providing these expressions not only clarifies the importance of DSI suppression, but gives a strategy for predicting performance for a particular scenario based upon the experimental benchmark results of the various algorithms.

Due to the importance of DSI mitigation techniques, there has been an appreciable amount of investigation in recent years. Predominant among these developments is the extensive cancellation algorithm (ECA) by Colone *et al.* [4], essentially a least squares (LS) technique generalized to incorporate Doppler-shifts of the reference waveform. In addition, variants of the CLEAN algorithm originally used in radio astronomy have also been proposed for PR DSI suppression [3], [5]. These methods, along with the typical LS algorithm, assume that the interference terms are fixed throughout the coherent processing interval (CPI), effects of which will be examined in Section IV. Many classical adaptive filtering techniques can also be adapted to remove PR interference, such as the normalized least mean squares (NLMS) algorithm, fast block least mean squares (FBLMS) algorithm, and recursive LS (RLS) algorithm [2], [6]–[8]. These adaptive algorithms will be shown to be less susceptible to degradation to time-varying clutter environments, due to their continually adaptive nature.

A few surveys to date have compared the effectiveness of various DSI suppression algorithms [6]–[9]. Cardinali *et al.* [9] compared least mean squares (LMS), NLMS, RLS, and ECA algorithms against simulated analog FM waveforms, but these results were not verified with experimental data sets. Suppression of the DSI was found to be approximately 50 dB. The ideal fixed clutter coefficients and signal structure of the analog FM modulation result in suppression benchmarks, which are not applicable to most modern digital signals in a realistic clutter and multipath environment. Palmer and Searle [7] conducted a survey comparing LS (Wiener) filtering, LMS, and RLS for digital video broadcast (DVB-T). The results show only 12–15 dB of reduction in the noise floor, far worse than the authors realized by any suppression algorithms under any circumstance. No insight is given to why the filters were performing in such a manner. This paper also did not include the FBLMS nor ECA algorithm, both of which will be shown to be highly performing algorithms with excellent suppression performance. In particular, FBLMS has received very little attention outside of the work in [8] and [10], but it will be shown that it is the most promising candidate among all compared algorithms for realizing real-time PR operation without sacrificing suppression performance.

This paper serves to unite the seemingly contradictory reports of performance in the literature for DSI suppression, and highlight the various underlying factors, which can degrade suppression performance. This comparison provides an overview and coverage of time-domain suppression algorithms and allow for an informed decision for selecting a DSI suppression strategy in the process of PR system design. The following algorithms will be compared on simulated and experimental digital television (DTV) data:

1) ECA;
2) LS;
3) CLEAN;
4) NLMS;
5) FBLMS;
6) RLS.

The DTV broadcast signals examined throughout this paper are specified by the Advanced Television Systems Committee (ATSC) A/53 standard [11], employed primarily across the North American continent in contrast to DVB-T used most commonly in Europe and Asia. The ATSC signal consists of an eight-level amplitude modulated signal, filtered to the upper sideband with a bandwidth of 6 MHz. Although ATSC waveforms are used here, the results are broadly applicable to any digitally modulated waveform, which has been processed to eliminate undesirable artefacts in the ambiguity function. The pilot tone was suppressed with a notch filter in the frequency domain prior to DSI suppression filtering to eliminate a zero-Doppler ridge in the ambiguity surface. If these operations are properly applied, the behavior of the algorithms and radar performance will be very similar to that of a random noise signal [5]. As such, the performance of the various suppression algorithms and related benchmarks should be generally consistent across other digital transmissions under similar conditions.

Section II is devoted to the fundamentals of the PR signal model, with relevance to the direct signal and clutter components. Range equations for the target, DSI, and thermal noise level of the surveillance channel are then developed. Section III is devoted to fundamentals of DSI filtering methods within the PR context. Section IV is an extensive evaluation of the various DSI suppression algorithms. An analysis of the primary factors affecting DSI suppression performance through simulated and experimental comparisons is first presented, followed by an extensive experimental validation across a wide range of DTV PR scenarios.

II. Passive Radar Signal Model

The basic signal models and PR RD processing will be explained here as an introduction to the problem of DSI suppression. Methods for calculating the effective DSI suppression can then be discussed, followed by range equations governing the magnitude of various components in the signal model and their relative strengths.

A. Received Signal Model

As mentioned previously, a PR system consists of a reference and surveillance channel for each illuminator of opportunity. The reference generally waveform collects a delayed

copy of the transmitted signal as

$$s_r(t) = A_r s_{\text{tx}}\left(t - \frac{R_L}{c}\right) + v_r(t) \tag{1}$$

where A_r is a complex amplitude term for the propagation effects of the transmitted waveform, $s_{\text{tx}}(t)$, which is delayed by the bistatic baseline range over the speed of light, R_L/c, shown in Fig. 1. This distance, as well as the transmit and receive locations, is generally assumed to be known and fixed for stationary PR systems. The additive white Gaussian noise is represented by $v_r(t)$. In practice, $s_r(t)$ is gathered with a highly directive reference antenna to maximize the signal-to-noise ratio (SNR) of the reference waveform, $E[A_r^2 s_{\text{tx}}^2]/E[v_r^2]$, where $E[\cdot]$ is the expectation operator. Due to finite realizable antenna beamwidths, the reference signal also contains some level of multipath and clutter, but this has been omitted for simplicity. The presence of clutter in the reference signal results in false peaks in the RD surface at closer ranges than the true distance to the scatterer (see Section IV-B for further discussion). If the effects of such components are significantly detrimental to performance, remodulation of the reference signal can be implemented [12]–[14], which can remove clutter, multipath, and noise from $s_r(t)$. Note that although these methods have only been demonstrated for DVB-T and ATSC waveforms, they can be extended to any digitally modulated waveforms whose signal structure is known, such as global system for mobile communication, DAB, WiFi, or WiMax. Unfortunately, this procedure adds computational overhead and care must be taken, such that the carrier-phase effects are properly accounted for to avoid degradation in the matched filtering process [14]. The signal must also have adequate SNR to be properly demodulated without significant errors, such that the reconstruction is accurate.

The surveillance waveform of a PR system consists of DSI (direct path, multipath, and clutter), Doppler-shifted target echoes, and thermal noise. The general form for the surveillance waveform, including these three components, can be written as follows:

$$s_s(t) = s_{\text{dsi}}(t) + s_{\text{tar}}(t) + v_s(t) \tag{2}$$

where $s_{\text{dsi}}(t)$ is the direct signal component, $s_{\text{tar}}(t)$ is the target signal, and $v_s(t)$ is noise. The DSI and target components are made up of scattered signals of $s_{\text{tx}}(t)$. Assuming that the waveform is observed over a sufficiently small interval, such that the Doppler-shifts can be treated as a constant, (2) can be expanded as

$$s_s(t) = \left[A^d(t)s_{\text{tx}}(t - R_L/c) + \sum_{p=1}^{P} A^p(t)s_{\text{tx}}(t - \tau^p)e^{j2\pi f_d^p}\right] + \sum_{q=1}^{Q} A^q s_{\text{tx}}(t - \tau^q)e^{j2\pi f_d^q t} + v_s(t). \tag{3}$$

$A^{(n)}$ represents the complex amplitude and phase terms for each component, representing both propagation effects and clutter/target radar cross section (RCS) values, where the superscript (n) is d, p, and q for the direct path, clutter, and target terms, respectively. The f_d terms represent the various Doppler shifts, proportional to their velocity relative to the bistatic bisector for the local target geometry [15]. Variables τ are the delay for each component, set by the bistatic range divided by the speed of light, $(R_T + R_R)/c$, as shown in Fig. 1.

The first two bracketed terms of (3) comprise the DSI: direct path/multipath breakthrough (generally the strongest signal) and P significant ground clutter responses, respectively. Note that the direct path breakthrough has the same delay as the reference, $s_r(t)$, with a known delay but unknown amplitude. In contrast, both the delay and amplitude of various clutter discretes are unknown and may possess a slight Doppler component, due to slight movement in the environment (e.g., trees swaying due to wind). Typically, this Doppler shift is less than the desired target Doppler, $f^p < f^q$.

Broadly, DSI suppression aims to estimate the first two terms of (3) in some fashion using knowledge of the transmitted waveform acquired through $s_r(t)$. This estimate of the DSI component can then be coherently subtracted from the surveillance waveform, such that the residual leaves only the target response and noise.

B. Power Calculations

The relative strengths of the various terms in (2) determine the degree of influence in which they impact PR system operations and performance. Modeling the power from a hypothesized target can be done by adopting the bistatic range equation, shown as follows:

$$P_{\text{tar}} = \frac{P_t^{\text{av}} G_t^{\text{tar}} G_r^{\text{tar}} \lambda^2 \sigma_b}{(4\pi)^3 R_T^2 R_R^2 L_t} \tag{4}$$

where the terms are as follows:

P_t^{av}	average transmitted power of illuminator of opportunity;
G_t^{tar}	gain of transmit antenna toward target zone;
G_r^{tar}	gain of surveillance antenna main beam;
λ	wavelength;
σ_b	bistatic RCS;
R_T	transmit range (transmitter to target);
R_R	receiver range (receiver to target);
L_t	losses (propagation and system) along target path.

Note that the bistatic RCS, for any particular target, is a complex parameter, which depends on RF center frequency, bistatic bisector, and bistatic angle, and can vary significantly, much as is the case for a monostatic RCS. Unfortunately, there is a lack of data in the open literature for realistic values of this parameter, but for complex targets at wide bistatic angles, the expected cross section may be significantly smaller, up to 10 dB, than that of the monostatic value [16]. The thermal noise power in the surveillance channel is the standard formulation of

$$P_n = kTBF \tag{5}$$

where k is Boltzmann's constant, T is the effective noise temperature of the receive antenna, B is the noise bandwidth, and F is the noise factor.

To adequately model the DSI terms, a combination of the Friis transmission formula and a summation of bistatic

radar range equations is required. This is due to the fact that DSI, in the most general form, consists of both direct path breakthrough into the surveillance antenna's sidelobes (one-way propagation) and strong multipath and clutter from the environment around the receiver (two-way propagation over various range and angles). These two terms, respectively, are shown in (6), and set the level of the amplitude coefficients of the bracketed term in (3)

$$P_{\text{dsi}} = \frac{P_t^{\text{av}} G_t^r G_r^t \lambda^2}{(4\pi)^2 R_L^2 L_d} + \sum_{p=1}^{P} \frac{P_t^{av} G_t^p G_r^p \lambda^2 \sigma_b^p}{(4\pi)^3 R_{T,p}^2 R_{R,p}^2 L_b} \tag{6}$$

where

G_t^r	transmit antenna gain toward the receiver;
G_r^t	surveillance antenna gain toward transmitter;
G_t^p, G_r^p	transmit and receive antenna gain toward pth clutter cell;
σ_b^p	bistatic RCS of the pth clutter cell;
$R_{T,p}$, $R_{R,p}$	transmit and receive range of the pth clutter cell.

Generally, the first term (direct path) of (6) dominates the power of the surveillance waveform. For PR systems with a fixed or adaptive antenna null in the direction of the transmitter, the direct path breakthrough may be weaker than some strong clutter components.

C. Passive Radar Processing

Now that the theory behind the signal model and power related calculations of a PR have been developed, the effects of signal processing can be examined. The fundamental stage of PR processing is computation of the RD map, from which target detection and tracking can be carried out directly. This surface is calculated via Doppler-shifted cross correlations of the reference and surveillance waveform in the form of the cross ambiguity function, shown as follows:

$$\Psi(R_D, f_d) = \int_{t=0}^{T} s_s(t) s_r^*\left(t - \frac{R_D}{c}\right) e^{-j2\pi f_d t} dt. \tag{7}$$

The RD map, Ψ, is calculated for hypothesized targets at bistatic range past baseline, R_D, and Doppler frequency f_d. In physical bistatic range terms, this can be viewed as $R_D = R_T + R_R - R_L$. R_D sets the correlation delay time, $t_d = R_D/c$. The Doppler frequency can also be used to calculate a target's bistatic velocity, $V = f_d \lambda$. Examples of RD maps for experimental PR data with ATSC waveforms are shown in Fig. 3.

DSI suppression is typically performed prior to RD processing, which reduces the power of the DSI term in the surveillance waveform by R_{dsi} dB—the focus of the Sections III and IV. In addition, the Doppler processing inherent in RD map formation can further separate moving target echoes from the stationary clutter and direct signal components. This is due to the thumbtack autocorrelation floor of noiselike digital waveforms at $10\log_{10}(\tau B)$ dB down from the zero delay and Doppler peak. This has been demonstrated for noise radar waveforms, ATSC, and DVB-T transmitters [5], [17], [18]. Therefore, the difference in the fully coherent integration of the target signal compared with the incoherent integration of the DSI (when mismatched at different delay and Doppler shifts of the target) and noise terms results in the following effective power levels relative to the target strength, shown as follows:

$$P_{\text{dsi\_eff}}^{\text{dB}} = P_{\text{dsi}}^{\text{dB}} - R_{\text{dsi}} - 10\log_{10}(\tau B) \tag{8}$$

$$P_{n\_\text{eff}}^{\text{dB}} = P_n^{\text{dB}} - 10\log_{10}(\tau B). \tag{9}$$

Note that for (8) and (9) to hold, the integration time, τ, must be sufficiently short, such that coherent integration of the desired target signal is maintained. This depends highly on the target kinematics, and integration time for a target with bistatic velocity V and radial acceleration A_r should be restricted to $\tau < c/VB$ or $\tau < (\lambda/A_r)^{1/2}$, which confines range and Doppler migration, respectively, to less than a resolution cell [1]. Effects of quantization noise can also be considered, but are typically negligible with the state-of-the-art analog-to-digital converters (ADC's) with a large number of bits [17], which can be further mitigated by oversampling [19]. Quantization can be modeled as an additional noise term also reduced by the same $10\log_{10}(\tau B)$ factor as the thermal noise and DSI. The ratio of the target power to interference terms can be used to calculate the surveillance antenna's signal to interference plus noise ratio (SINR), which reveals the expected radar performance for a particular scenario

$$\text{SINR} = \frac{P_{\text{tar}}}{P_{\text{dsi\_eff}} + P_{n\_\text{eff}}}. \tag{10}$$

The goal of DSI subtraction is to reduce the effective DSI contribution by a sufficient amount, such that the in-band thermal noise floor remains the limiting factor, which can only be suppressed via matched filtering of the reference waveform. At such point, increasing the SNR in the radar must be gained by alternative methods of increasing the receive antenna gain, minimizing the noise figure and losses in the receive chain, or by extending the length of the coherent integration gain if possible.

Fig. 2 shows the general relative power levels of the direct signal, noise, and target signal in the surveillance waveform. The power levels are described in the preceding equations, the arrows represent stages of processing and shielding, and the dashed lines illustrate the range of power levels often seen by PR systems. The top of the first column, representing the direct signal power, begins with the power in the reference signal of a PR receiver, P_{ref}, often with a directive antenna toward the illuminator. Physical isolation (null-steering or sidelobes oriented toward the transmitter, polarization mismatch, or shielding) further decreases the DSI power received by the surveillance channel relative to the reference. The level of P_{dsi}, P_n, and P_{tar} represents the power levels that digitized by the PR receiver. The DSI is then further mitigated by the DSI suppression factor, R_{dsi}, due to the time-domain processing. When the RD map correlation is matched to a particular target's range and Doppler position, the target signal experiences a large coherent integration gain compared with the unmatched terms: noise and DSI (which is only integrated at the zero Doppler position). The net effect of the correlation processing is, therefore, a relative reduction in the

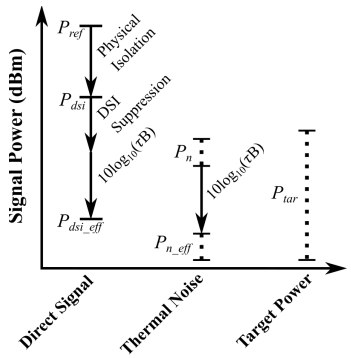

Fig. 2. Illustration of DSI power levels and suppression.

DSI and noise terms by the time bandwidth product compared with the full integration experienced by the target signal.

The maximum possible DSI suppression, if measured from the reduction in the RD map noise floor, corresponding to complete elimination of the direct signal terms, such that only the target signal and noise remain is given by the interference-to-noise ratio

$$\mathrm{INR} = \frac{P_{\mathrm{dsi}}}{P_n}. \tag{11}$$

D. Practical Calculation of DSI Suppression

The effectiveness of DSI suppression must be established by proper choice of metric. Cardinali *et al.* [9], [20] have evaluated the DSI suppression by the ratio of powers in the surveillance waveform before and after suppression. However, it was found through experimental testing conducted in the presented research that this method of calculation is not reliable for estimating the effective reduction of the noise floor in the RD map, and resulted in overestimation in a suppression of 3–5 dB from many empirical observations. By computing the RD surface twice (prior to and after DSI suppression), the effective DSI reduction can be directly calculated, allowing for accurate estimation of R_{dsi}.

The portion of the RD map isolated for the DSI suppression value is shown in Fig. 3(a) and (b) bounded by the rectangular box. The region of the RD map selected excludes any significant clutter contributions, as well as that of strong target responses, seen in Fig. 3(b) after the application of DSI suppression. All powers shown in the various subplots are consistent and measured relative to the direct signal power of the reference waveform. The effective value of DSI suppression is found by computing the average of the dB values between Fig. 3(a) and (b), which minimizes the estimate of the floor level to erroneous data points, such as a target above the noise floor. Notice the strong target circle in Fig. 3(b) was completely masked by the sidelobes of the DSI terms on the zero-Doppler line of Fig. 3(a) prior to subtraction. The SINR for a given target can be calculated as the target's peak response divided by the average power in the rectangular border.

Fig. 3(c) and (d) shows the zero-Doppler cut through the RD maps shown in Fig. 3(a) and (b). The 1000 filter taps of the LS filter used for suppression show excellent cancellation of

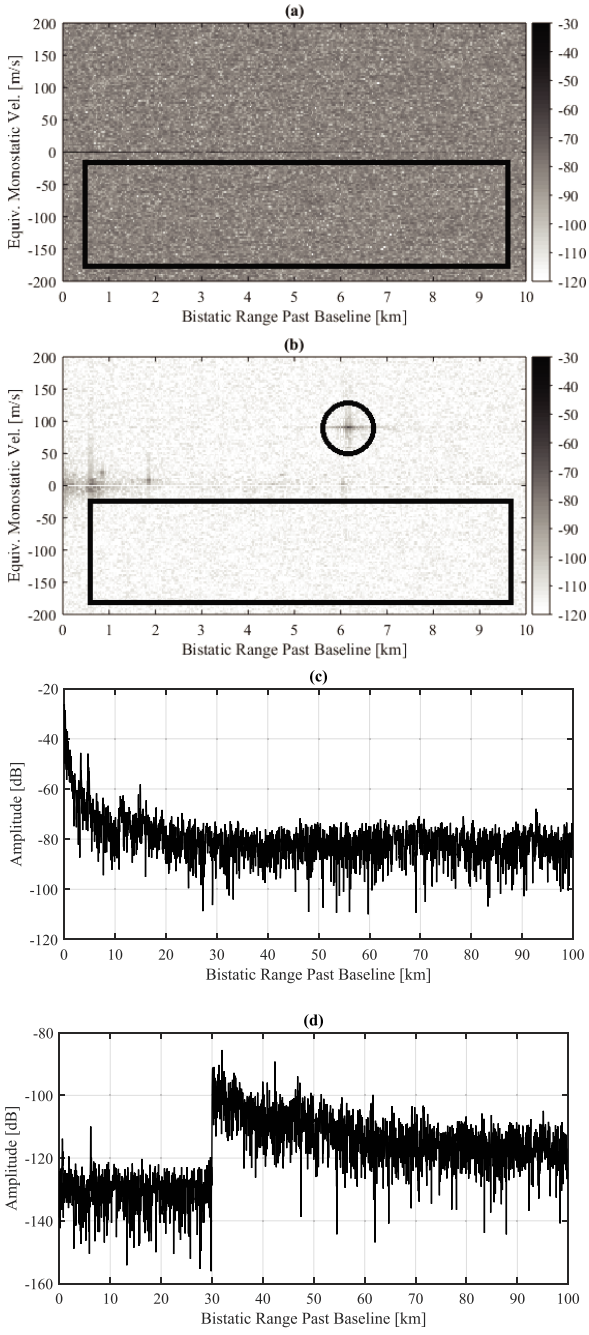

Fig. 3. Illustration of LS DSI suppression on experimentally collected ATSC data. (a) RD map prior to suppression. (b) RD map after suppression. (c) Zero-Doppler cut of (a). (d) Zero-Doppler cut of (b).

the clutter to 30 km, suppressing the direct signal breakthrough and clutter by up to 80 dB. The effective noise floor is also reduced by about 35 dB, far less than the reduction in the zero-Doppler clutter. Notice that the cancellation of 1000 coefficients revealed not only the target of Fig. 3(b), but also residual clutter components beyond 30 km, which also previously masked by the direct signal breakthrough.

III. DSI Suppression Fundamentals

This section focuses on the basic model for DSI suppression along with a brief overview of the various algorithms to be compared in Section IV, along with practical implementation considerations.

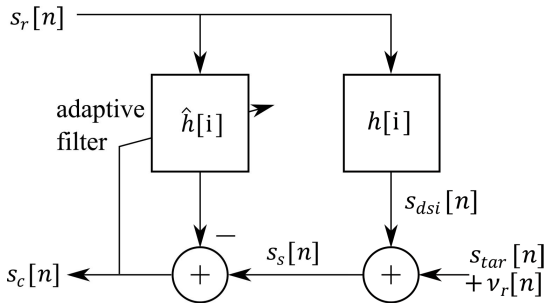

Fig. 4. Block diagram for DSI suppression.

A. Framework for Adaptive Filtering

The general model for adaptive filtering, tailored to the DSI suppression problem, is shown in Fig. 4. Because these algorithms are implemented via digital signal processing after digitization with an ADC, the terms are shown here with square brackets to indicate discrete time, sampled at interval T_s, such that $t = nT_s$. The reference waveform passes through an finite-impulse response filter with impulse response $h[i]$, representing the delay and complex scattering coefficients of the DSI

$$s_{\text{dsi}}[n] = \sum_{i=0}^{M-1} h^*[i]s_r[n-i] \tag{12}$$

where M is the number of discrete time delay coefficients to properly model the maximum bistatic range of the DSI components greater than the noise power, $M = \lceil R_D^{\max}/cT_s \rceil$, where $\lceil\cdot\rceil$ is the ceiling operator. The various discrete samples of $h[i]$ represent a continuum of clutter responses, and as such, it is inevitable that many clutter responses will arrive at a time delay corresponding to a fractional number of ADC sampling periods. Typically, a response for a given clutter discrete will be spread across neighboring coefficients of $h[i]$ with reduced amplitude [21].

The DSI removal process first estimates the unknown clutter and direct path coefficients, $\hat{h}[i]$, and then convolves the result with the reference channel waveform to estimate $s_{\text{dsi}}[n]$. This output is subtracted from $s_s[n]$ to leave only target responses and thermal noise in surveillance signal. The final output after these operations is represented by $s_c[n]$, a DSI-free "clean" surveillance channel consisting of the target response with additive noise.

While relatively weak clutter responses (compared with the direct path leakage A^d) may have a negligible impact on the total DSI power in the surveillance waveform prior to suppression (6), their power is often significantly greater than thermal noise and will thus degrade the SINR if not accounted for. The effectiveness of the DSI subtraction process degrades if M is insufficient to properly model the clutter response, but computational requirements are relaxed as M decreases. Effects of varying the number of coefficients of $\hat{h}$ will be further examined in Section IV.

B. DSI Mitigation Algorithms

Methods of digital filtering for DSI suppression can be classified by two primary categories, adaptive filtering and fixed coefficient filtering. Conventional classification for adaptive filtering approaches groups schemes into two primary groups: block and fully adaptive methods. Fully adaptive methods update the filter coefficients $\hat{h}[i]$ for each fast time sample n throughout the processed CPI, while methods which update the coefficients every N samples are referred to as block methods. Typically, $N = M$, the same length as the number of filter coefficients in $\hat{\mathbf{h}}$, significantly smaller than the number of samples in a typical CPI for PR that is usually at least 100 ms [22], requiring upward of one million samples. For this paper, a filter whose coefficients are updated within a CPI (both fully adaptive and block methods) shall be classified as adaptive, whereas filters which select a single set of coefficients for the entire CPI shall be referred to as fixed coefficient filtering methods.

Of the compared algorithms, LS, ECA, and CLEAN are categorized as fixed coefficient methods, while NLMS, RLS, and FBLMS are adaptive filtering techniques. Fixed coefficient filtering techniques assume that the joint statistics of the reference and surveillance waveforms are wide-sense-stationary over the CPI, which may not hold in practice due to time-varying clutter environments and receiver system antenna motion and instabilities. The adaptive techniques, in contrast, can automatically adjust to time-varying signal statistics, which can cause degradation of the suppression performance if not properly accounted for. Investigations into this will be discussed in Section IV.

Details of the algorithms are well documented and thus outside the scope of this paper, the reader should refer to the following references for the detailed theory of the following algorithms: the CLEAN algorithm was developed by Kulpa [3], Kulpa and Czekała [5], and the ECA by Colone *et al.* [4], while the procedures for LS, NLMS, RLS, and FBLMS are derived in detail by Haykin [2].

1) Remarks on Implementation: For this paper, the ECA has been implemented in a single stage by directly solving for the optimal clutter coefficients to project the surveillance signal into the orthogonal subspace to the clutter subspace, as in [4, Sec. III], $\hat{h} = (\mathbf{X}^H\mathbf{X})^{-1}\mathbf{X}^H\mathbf{s}_s$, where $\mathbf{X}$ is a matrix of time-delayed, Doppler-shifted replicas of the reference waveform. Although there exist batch methods as well as iterative subtraction algorithms to remove strong clutter and targets, the direct implementation was used to permit more straightforward comparison with other algorithms. Regarding implementation complexity, calculating the autocorrelation matrix ($\mathbf{X}^H\mathbf{X}$) and cross correlation vector ($\mathbf{X}^H\mathbf{s_s}$) directly with FFT correlation methods was found to significantly reduce memory and computational requirements.

The CLEAN algorithm was also implemented using only a cross correlation of the reference and surveillance, without compensating for Doppler shifted target echoes, as proposed by Kulpa and Czekała [5]. A similar approach, which suppressed zero-Doppler clutter, has been proposed for through-wall sensing [23]. This method used interpolation in range for the subtraction stage, but it was found that this additional step was an unnecessary addition as it did not improve suppression significantly. It will be shown in the remainder of Sections III and IV that without interpolation, much improved suppression

values were achieved compared with the average 19 dB of suppression [23].

The NLMS algorithm was chosen rather than that LMS algorithm due to the normalization factor in the adaptive algorithm, which eliminates hand-tuning the adaptation parameter, μ, for each illuminator due to the various signal strengths. An alternative would be to normalize the energy of reference signals prior to DSI processing, which would permit a single optimized parameter for all signals.

Difficulty in optimizing implementation varies considerably between the algorithms, primarily due to the different number of parameters for each method. The LS algorithm finds the filter coefficients $\hat{h}[i]$, which minimize the squared error signal, $s_c[n]$. LS has no tunable parameters, and thus gives a single solution for a particular CPI, which makes it straightforward to implement. ECA generalizes this operation for Doppler-shifted versions of the reference waveform, but still assumes that the magnitude and phase remain constant throughout the processing interval. However, the ECA has the additional choice of the number of Doppler bins (and delays) to suppress outside the zero-Doppler clutter region.

The NLMS and RLS algorithms have only one single adaptive parameter, which controls the coefficient update rate. FBLMS, on the other hand, has two tunable parameters, which affect the convergence and performance of filter [2]. It was found that setting the frequency domain parameter $\gamma = 1$ for FBLMS allowed for convergence to be achieved without too much difficulty. An additional energy normalization factor[1] was also included, taking inspiration from NLMS, which allowed for a single, common adaptive parameter to be used across all experimental and simulated data sets. This approach, developed during the experimental analyses of Section IV-B, was not found in the literature but was found to work well in practice.

Assuming the CPI is fixed to a particular length, all filtering schemes require common input in terms of the number of coefficients of the estimated direct path and clutter coefficients, $\hat{h}[i]$. The number of suppression iterations for CLEAN algorithm can be viewed as the counterpart to the number of filter taps for the other methods. The number of filter taps for optimal performance must be estimated based upon experimentally collected data, due to the dependence on the clutter distribution seen by the surveillance antenna. In all cases, there is a definite tradeoff between the number of filter taps and computation requirements for all algorithms, as will be investigated in Section IV-A.

IV. Evaluation of DSI Suppression

A. Factors Affecting Suppression

Aside from the choice of suppression algorithm, there are numerous factors, which influence suppression performance. From extensive simulation and experimental analyses conducted here, the primary factors can be grouped into external effects as well as intrinsic processing parameters. External factors affecting suppression have to do with the signal purity (amount of multipath and SNR) of the reference and surveillance waveforms, as well as the physical clutter environment and its stationarity. The choice of processing parameters involves not only the choice of suppression algorithm and its tunable coefficients, but also the CPI over which the data is to be processed.

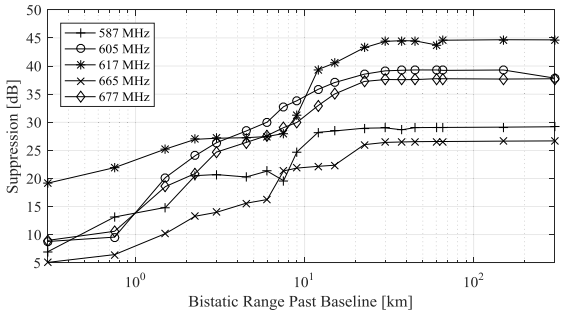

Fig. 5. LS suppression versus filter length for all illuminators.

1) Channel Length: Most broadcast illuminators for PR exhibit high power levels and near omnidirectional beampatterns slanted toward primary users on the ground. This results in a large number of strong clutter components over a wide swath of bistatic ranges and angles. Thus, a given DSI filter must have an adequate number of taps to sufficiently suppress the zero-Doppler clutter ridge in bistatic range until the clutter power decreases past the thermal noise, the theoretical maximum effective suppression of (11). Results of suppression versus bistatic range are shown in Fig. 5, plotted for many experimentally measured DTV illuminators using the LS algorithm. Details of the experimental setup for these results are given in Section IV-B. Notice that the suppression of the effective noise floor stabilizes after approximately 30 km in bistatic range, although clutter coefficients remain above the noise floor shown in Fig. 3. However, the shapes of the curves vary due to clutter distribution between each transmitter. Notice that significant clutter is seen beyond 30 km in Fig. 3, but suppressing these causes no further reduction of the effective noise floor in the RD map. The cause of this effect can either be attributed to residual components of the stronger direct path breakthrough due to imperfections in the DSI mitigation algorithm, or the thermal noise floor in the surveillance channel, as will be further investigated in Section IV-B.

2) Signal Purity: Three predominant factors comprise signal purity—SNR of the reference waveform, INR of the surveillance waveform, and the presence of clutter or multipath in the reference channel. For PR systems with minimal reference clutter (using moderately directive reference antennas and line of sight to the illuminating source), the effective suppression level is bounded by the lower of either the reference SNR or the surveillance INR. In practice, the reference SNR is typically higher due to the directive antenna beam pointed straight toward the transmitter. Therefore, the thermal noise in the surveillance channel is most often the limiting factor for performance.

[1]The normalized version of the FBLMS, where the true update coefficient, consistent with [2] is $\alpha = \mu \cdot 4000 \cdot E[s_r^2(n)]$. This normalization constant typically converges within the range of $0 < \mu < 1$, a similar range to the behavior of the NLMS algorithm.

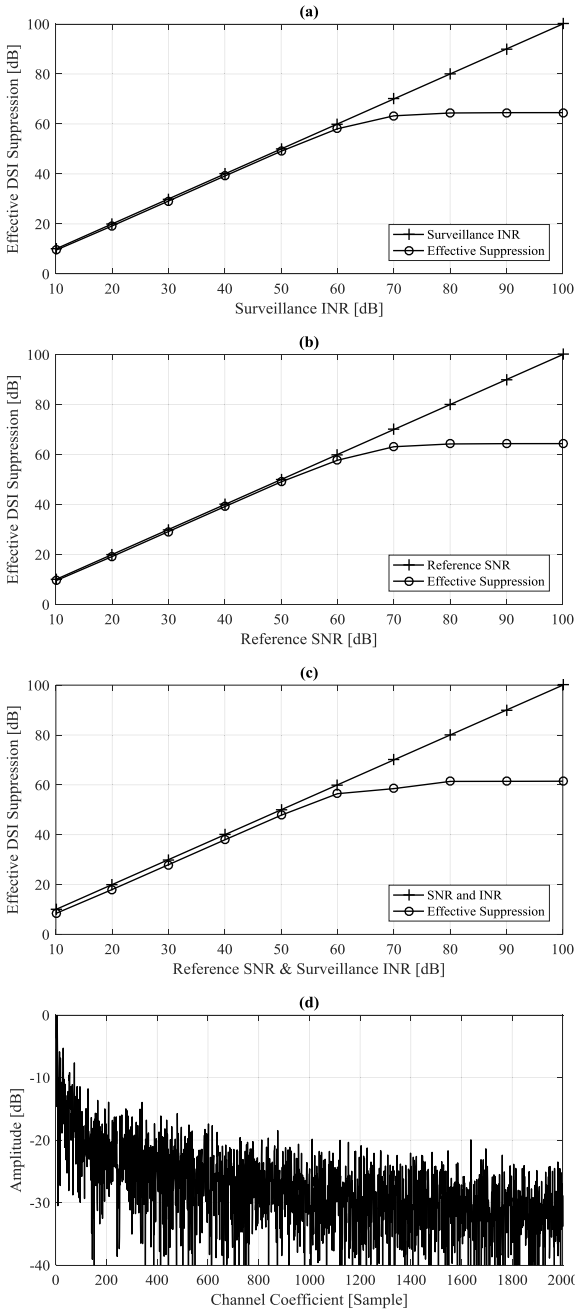

Fig. 6. (a) Suppression versus surveillance INR. (b) Suppression versus reference SNR. (c) Suppression versus SNR and INR. (d) Simulated random channel coefficients.

Fig. 6 shows the results of simulation analysis demonstrating suppression performance as a function of both INR and SNR. A 6-MHz bandlimited noise waveform was generated to represent the transmitted waveform. The direct path and clutter coefficients, $h[i]$, were modeled as complex Gaussian random variables whose variance decreased by factor $(1/\text{index})^{0.25}$ to represent the $1/R^4$ spreading losses of the radar. This clutter vector is shown in Fig. 6(d). These coefficients were convolved with the reference waveform to generate an ideal surveillance signal representing a stationary clutter environment throughout the CPI.

Results of Fig. 6(a) show suppression as a function of surveillance INR, with a noise free reference signal. For this ideal case, the DSI can be very well estimated, but the noise remains after filtering and sets the noise floor of the RD map. In Fig. 6(b), the reference SNR was varied and suppression applied to a noise free surveillance signal. In this case, the noise is added to the surveillance waveform as a side-effect of the DSI subtraction process, which is shown to limit the suppression performance in a matter somewhat analogous to the surveillance INR case. For the case where noise was added to both the reference and surveillance simultaneously of Fig. 6(c), the mitigation performance degrades further by approximately 2–3 dB due to the additive noise effects between both channels. These results also show an upper limit of the LS algorithm of around 64 dB of suppression for an ideal linear and stationary clutter environment.

A complete treatment of reference signal clutter is outside the scope of this paper. The presence of strong specular scatterers with additional time delay of t_c relative to the direct path results in noncausal ambiguities from the direct path and false targets at a range of $R_{\text{tar}} - ct_c$, where R_{tar} is the true bistatic range to the target. As mentioned previously, these disturbances can be removed for digital modulations through remodulation procedures at a slight increase in computational requirements. Another method for mitigating noncausal clutter ambiguities is to delay the surveillance waveform prior to DSI suppression [21]. It was found that 0.5-dB improvement could be achieved in practice for FBLMS for ATSC by delaying the surveillance waveform up to 10 μs (100 samples at 10 MSa/s), but no significant improvement was seen for the other algorithms. This was attributed to the FBLMS's adaptive component operating in the frequency domain, rather than the time domain of the other algorithms.

In addition, target echoes intended for the surveillance channel may appear in the reference channel causing additional range- and Doppler-shifted RD peaks. For a target at range and Doppler coordinates of $(R_{\text{tar}}, f_{\text{tar}})$, a secondary peak will appear at $(-R_{\text{tar}}, -f_{\text{tar}})$ due to correlation of the leaked target echo with the direct path. A more unfortunate consequence of these phenomena is the disturbance in the target signal, which occurs due to the subtraction processes inherent in DSI suppression, where the worst case is complete cancellation of the target signal. Although unlikely, this would occur when the relative amplitude and phase of the leaked target signal between the reference and surveillance channels were equal to that of the first, direct-path leakage coefficient in the estimated DSI channel. For geometrical scenarios where target responses are strongly received by the reference channel (which will most likely occur in the direction of the bistatic baseline), the demodulation operations above would be necessary for reliable operation and estimates of the target's echo strength unless a secondary remote receiver is available for reference sampling.

Close, strong Doppler-shifted target responses greater than the noise floor in the surveillance channel behave as an additional interference terms and can also limit suppression performance. A number of methods have been proposed to mitigate these effects [4], [5], [21], [24]. However, the focus of this paper is on clutter and direct path suppression, and as

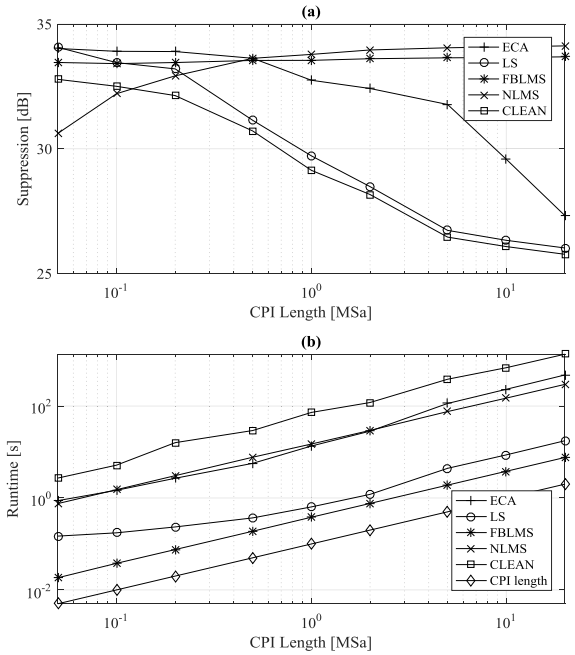

Fig. 7. Suppression versus CPI Length with 1000 filter taps (30 km). (a) Suppression of the RD noise floor. (b) Runtime in seconds versus CPI length.

such, all results are presented in the absence of strong target responses, which limit the PR sensitivity.

3) CPI Length and Clutter Stability: Long CPI's often result in degradation of DSI suppression performance with fixed-coefficient filtering methods, even for a stationary PR system and illuminator. This behavior is attributed to the nonstationary behavior of the clutter coefficients, which vary slowly due to moving clutter (trees swaying) and antenna motion. The resulting phase changes throughout the CPI will cause mismatch in the true and estimated channel coefficients, resulting in impartial subtraction of the DSI component. Although a fixed coefficient method (LS or ECA) may return the optimal solution for minimizing the squared error signal for the entire CPI, the result is not guaranteed to be the exact channel coefficient when localized to a particular instant in time.

Fig. 7 demonstrates the degradation in suppression of up to 8 dB for extended CPIs, due to the real-world phase variations of the channel coefficients. These results were computed using a single experimental ATSC illuminator, consistent with experimental trials of Section IV-B. Notice that the adaptive algorithms (FBLMS and NLMS) experience constant performance or improve with CPI length (due to longer training sequences and better coefficient estimation), whereas the fixed coefficient methods degrade as the processing interval lengthens. In order to sufficiently suppress these time-varying components, adaptive algorithms must be selected and tuned to properly track the slowly moving objects and clutter, which are not of interest to the radar.

The runtimes of Fig. 7(b) show that all algorithms have runtimes exceeding the CPI length when computed with MATLAB on an Intel Xeon E5-2687W octa-core processor. Notice that all runtimes are proportional to the CPI length, except for LS, where the runtime remains high for short CPIs. This is due to the inversion stage of the cross correlation matrix of set by M, rather than the processing interval. Significant effort was made to reduce the runtime of each algorithm within the MATLAB framework where possible. Runtimes for the adaptive algorithms do not include the training period to converge to locally optimum coefficients at the start of the CPI. Since all algorithms exhibit runtimes greater than the CPI length, a simple serial implementation cannot provide uninterrupted update rates without further effort to decrease the computation time, such as implementation on a field-programmable gate array or dedicated DSP board. Allowing for processing latency, a similar system could provide continuous update rates at the same interval as the CPI assuming Q parallel processing chains can be employed, where $Q = \lceil T_{\text{Proc}}/T_{\text{CPI}} \rceil$.

4) Adaptive Parameters and RD Null Width: Adaptive filters are typically designed to minimize the mean-square error signal, $s_c[n]$, and therefore, high performing (fast convergence) filters, such as RLS, generally achieve very low error. However, because of the convergence properties of the filter, an appreciable Doppler null will be created in the RD map. The adaptation parameter and behavior determines the width of the low-pass filter characteristic of the clutter estimation, s_{dsi}, which is then subtracted to generate the cleaned surveillance signal [21]. Because the filter is not intelligent enough to discriminate targets of interest from clutter, any target signals will also be removed. The highly adaptive nature of the filter results in subtraction of the $s_{\text{tar}}[n]$ component of $s_s[n]$ of Fig. 4. Careful consideration of the DSI suppression scheme's adaptive coefficients should be taken to ensure the Doppler null is sufficiently wide to remove the dominant stationary and slow-moving clutter but retain signals from targets at low velocity.

The application should also be considered when selecting and tuning an adaptive algorithm, due to the varying widths of the Doppler null in the RD map. Using the fixed coefficient algorithms applied full CPI (rather than the batch processing method of [4]), only a single line of Doppler pixels will be suppressed, because the filter taps are fixed over the entire processing interval. For the case where slow-moving targets are of interest, this would be desired. However, if only fast-moving targets are of concern, a fully adaptive algorithm would be a preferential subtraction scheme due to the adaptation to time-varying clutter effects. Fig. 8 shows the RD map and the Doppler cuts of the LS and FBLMS suppression schemes. The cuts of Fig. 8(c) and (d) were the averaged over a number of range bins where the DSI component was suppressed. Increasing the adaptive parameter of the various adaptive algorithms (NLMS, FBLMS, and RLS) results in faster convergence but also a wider LPF bandwidth for the filter coefficient estimation [21], which creates a larger null in the RD map after subtraction in which detection performance would suffer.

By tuning the adaptive filter parameter to track the Doppler spread from the time-varying direct path and clutter coefficients, optimal suppression can be achieved. However, the adaptive parameter also sets the rate of initial convergence

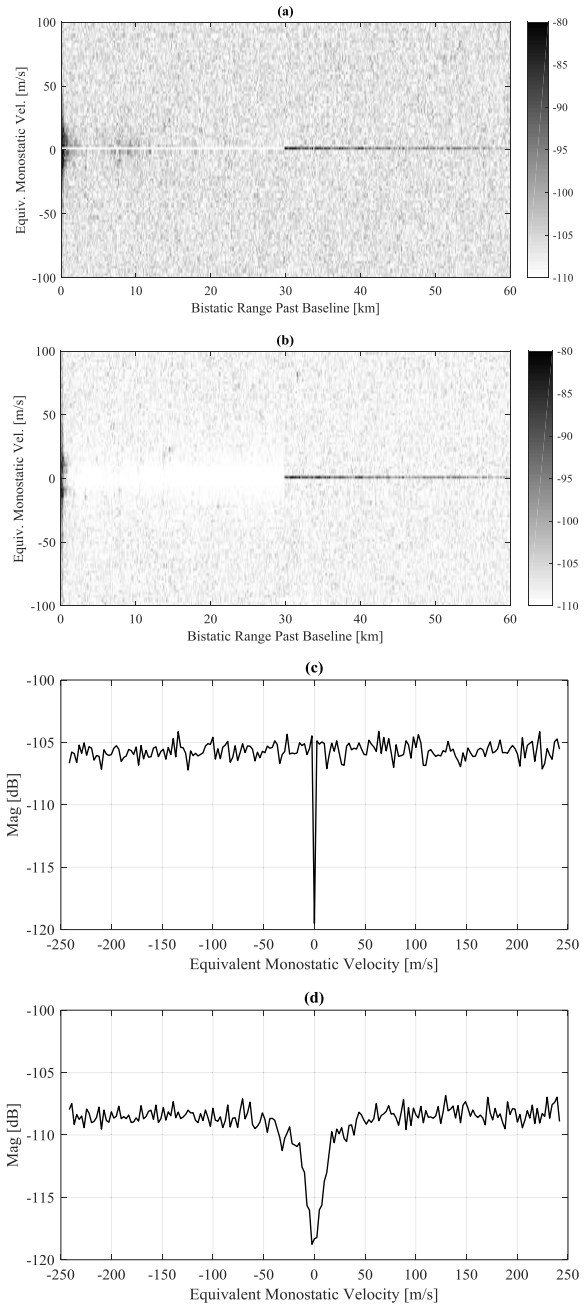

Fig. 8. Null width of fixed-coefficient and adaptive algorithms. (a) LS filter RD map. (b) FBLMS filter RD map. (c) LS mean zero-Doppler cut through null. (d) FBLMS mean zero-Doppler cut through null.

at the start of the CPI in which only partial clutter cancellation occurs unless the DSI filter coefficients, $\hat{h}[i]$, are initialized close to the true values of $h[i]$. For a fixed data length, this limits the coherent integration time as the initial data must be discarded to avoid a higher interference level due to the presence of DSI terms. For implementation with PR systems generating sequential RD snapshots where continuous operation of the adaptive filter is prohibited, there are two primary methods of channel filter initialization: first, the final estimate of the channel coefficients from the previous CPI can be used [7]; second, an initial training period can be performed by iterating through the first few milliseconds of a CPI with a highly adaptive filter coefficient until the clutter coefficients have stabilized. The resulting estimate of $\hat{h}[i]$ is then used and applied to the full CPI, with a reduced adaptation parameter set to the desired width of the Doppler null in the RD map. This procedure yields a good estimate of the initial channel coefficients, can operate on a single CPI and minimizing training time (due to the increased adaptation rate), and as such was implemented to generate the results of the adaptive filters in this paper.

5) Other Factors: Recent publications have proposed methods for dealing with fractional delays resulting from clutter delays for noninteger multiples of the sampling frequency [21], [25]. It is clear that due to natural displacement of the reference and surveillance antenna, as well as the continuum of clutter discretes, that any experimental system will contain many fractionally delayed components. However, it was found that the impact of this behavior resulted in negligible degradation in DSI subtraction performance for all algorithms (<1 dB). In the time domain, a fractional delay manifests as two clutter coefficients in the adjacent range positions [21]. The FBLMS performs the correlation in the frequency domain directly, which can also directly compensate for fractional shifts of the clutter distribution.

Distortions of the signals can arise through reflection, propagation, and reception of the signals in both the reference and surveillance channels. These distortions, if not equivalent for both the reference and surveillance channels, will cause a mismatch between the true and estimated DSI components, causing residual DSI prior to subtraction operations. RF and ADC design for PR systems should prioritize linearity to minimize these effects. Unfortunately, this behavior is difficult to measure or predict in practice.

B. Experimental Validation

This section investigates suppression performance for the DSI suppression algorithms discussed in this paper on experimental ATSC PR data, using a variety of illuminators and PR geometries. The data were collected in five different measurements spaced throughout three days. Each measurement consisted of a five second record interval. Results in this section reveal the behavior of suppression performance over system operational times, and validate some of the factors affecting DSI suppression presented in Section IV-A5. Results herein are applicable to any digital illuminator of opportunity, which possess similar noiselike ambiguity performance.

1) Experimental Setup: All experimental data contained herein were gathered with the MUltistatic digital TElevision passive RAdar at The Ohio State University's ElectroScience Laboratory, located in Columbus, Ohio [18]. This wideband UHF system collects the DTV spectrum from 580–680 MHz and, therefore, measures a number of different transmitters and real antenna beams, as shown in Fig. 9. Each transmission was digitally downconverted separately with a final 10-MHz sampling frequency, to satisfy Nyquist with sufficient margin for optimal performance with slight additional computational overhead. The geographical spread in transmit sites for the collections is shown in Fig. 9(a), and the transmit parameters are listed in Table I, all of which broadcast with horizontal

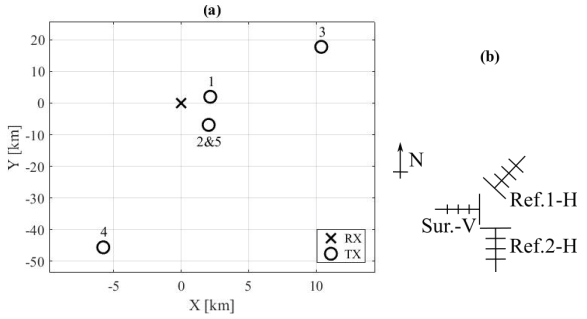

Fig. 9. (a) Illuminator geometry. (b) Receiver antenna configuration.

TABLE I
TRANSMITTER PARAMETERS FOR FIG. 9

Transmitter Index	Center Frequency [MHz]	Baseline [km]	Power [kW]
1	587	2.9	15
2	605	7.2	1,000
3	617	20.6	503
4	665	45.9	1,000
5	677	7.2	1,000

linear polarization. The wide range of bistatic baseline distances, center frequencies, angular spread, and transmit power result in a rich data set that can be analyzed to thoroughly evaluate the DSI suppression performance of the various algorithms from Section II.

Fig. 9(b) demonstrates the antenna configuration, consisting of two dedicated reference Yagi antennas, copolarized to the reference signal. The surveillance antenna was facing West, roughly 90° away from the transmitters of opportunity, polarized vertically (cross-pol) for reduction in the DSI breakthrough.

2) Suppression Performance With 100-ms CPI: This section analyzes the DSI suppression performance of the various algorithms for a general PR scenario observing air targets. A 100-ms CPI is used here, corresponding to the maximum length for coherent integration gain for air targets up to 250 m/s with the 25-m range resolution of ATSC waveforms. The data is sampled at 10 MSa/s after digital downconversion, resulting in 1-MSa data per processing interval. To directly compare the results of the various DSI mitigation techniques, the parameters of each algorithm were individually tuned to maximize the effective suppression between the various illuminators. The adaptive filtering methods (NLMS, FBLMS, and RLS) were set to maintain a -3-dB Doppler null, relative to the noise floor after subtraction, within ± 100 Hz, or ten Doppler bins for the CPI and sampling parameters. This null corresponds to an equivalent monostatic target velocity of less than 25 m/s at 600 MHz. The optimized parameters for each filter are shown in Table II. All filters used 1000 coefficients, equivalent to 30-km bistatic range past the baseline, where the suppression stabilized as a function of filter length across the various illuminators and algorithms (see Fig. 5).

TABLE II
DSI FILTERING PARAMETERS AND RUNTIMES

Algorithm	Parameters	Runtime [s]
No Suppression	N/A	0.0
ECA	3 Doppler bins 50 range bins	12.5
LS	N/A	0.64
FBLMS[1]	$\mu = 0.1$ $\gamma = 1$	0.38
CLEAN	1,000 iterations $\alpha = 0.95$	72.5
NLMS	$\mu = 0.09$	15.2
RLS	$\mu = 1$	>1 day

The runtimes for the one million sample CPI and 1000 estimated channel coefficients, $\hat{h}[i]$, are shown in the final column, calculated with MATLAB on the Intel Xeon E5-2687W octa-core processor, as in the discussion of Fig. 7(b). The results of the runtime tests show that both the FBLMS and LS algorithms represent good candidates for real-time implementation, with runtimes of less than 1 s. It may also be possible to further improve the speed of LS filtering by exploiting the toeplitz nature of the autocorrelation matrix, $\mathbf{X}^H\mathbf{H}$, for the matrix inversion procedure [2], which was not performed here. Due to the excessive runtime of RLS and no apparent benefit over the other adaptive algorithms, the filter will be discarded from further comparisons. Faster (albeit more complex) implementations do exist, but the computational requirements still remain significantly higher than NLMS, which had a runtime 150 times that of the CPI. In addition, the fast convergence rate of RLS forced the adaptive parameter to unity, $\mu = 1$, to avoid a large null in the RD map effectively attenuating targets at all Doppler frequencies in the RD map. Compared with the other algorithms under such conditions, the RLS filter did not demonstrate any benefit for any other metric.

Suppression results for all remaining algorithms (ECA, LS, CLEAN, NLMS, and FBLMS) across the various illuminators and collections are shown in Fig. 10. The five measurements of five seconds each were processed at intervals of 0.25 s, such that the start of each CPI for all measurements was $(0, 0.25, 0.5, \ldots, 4.75)$ s, respectively, for a total of 20 suppression datapoints for each filter across the five simultaneous received ATSC signals of Fig. 9. In total, 100 values of suppression were tallied for each algorithm and illuminator pairing, but the data are shown downsampled by a factor of 2 for illustration purposes. In addition, the tabulated mean and variance (of the decibel suppression values) are shown in Table III, sorted by algorithm and illuminator center frequency. Notice that the second and third rows of Table III shows the reference signal SNR and the surveillance INR, measured by replacing the antenna feed with a matched load and calculating the power spectral density of the in-band noise signal. The ratio of the signal power to this noise power calculates the SNR and INR values for the reference and the surveillance channel.

From analysis of Fig. 10, it is clear that there is a general trend for some filters to outperform the others. In general,

TABLE III
(LEFT) MEAN AND (RIGHT) VARIANCE IN SUPPRESSION [dB]

Fc [MHz]	587		605		617		665		677	
Reference SNR [dB]	50.7		66.4		60.3		36.6		65.2	
Surveillance INR [dB]	41.3		61.2		56.1		34.1		62.5	
ECA	33.3	3.5	41.8	3.6	47.2	2.4	27.6	5.8	40.6	3.8
LS	31.5	2.7	38.2	5.2	43.6	12.1	27.6	2.7	37.5	3.1
FBLMS	33.9	0.6	42.3	0.5	47.9	0.2	27.8	1.2	42.1	1.1
NLMS	33.8	0.9	42.0	7.3	47.4	2.4	27.9	1.2	41.3	5.6
CLEAN	31.0	1.0	34.9	0.4	42.5	1.0	27.5	1.3	35.9	1.5

the adaptive algorithms of FBLMS and NLMS and the ECA exhibited the highest levels of suppression. The two lower performing algorithms, purely based upon suppression performance, are the LS method and the CLEAN algorithm. Because of high computational cost of the CLEAN algorithm, coupled with the fact that the suppression was comparatively poor, it will not be discussed further here as there is no distinct advantage of the technique. The LS algorithm, on the other hand, was the second fastest algorithm of all tested, which merits further discussion and investigation.

From inspection of Table III, note that the reference SNR is higher than the surveillance INR. This is due to the cross-polarized surveillance antenna and different RF architecture of the reference and surveillance channels. In general, the effective suppression is approximately 10–20 dB less than the surveillance channel INR. It would appear that as the INR increases, the gap between the suppression and the INR widens slightly. Notice that the 665-MHz results of the furthest illuminator, where the reference signal was likely not as pure as the closer range transmitters resulting in the lower SNR and INR, exhibited close to the same performance for all algorithms, and an effective noise floor only 6 dB away from the thermal noise level. The stairstep function, which transitions every 20 CPIs (for each measurement) shows that some unknown environmental effects occurred in the hours between collections, which impact the effective suppression value. This could be due to changes in propagation due to weather or varying quality in the reference signal purity.

These results show that the state of the art of PR systems is not capable of reaching the receiver's thermal noise floor, solely relying on a time domain DSI approach and real-beam antennas. The cause of this could either be attributed to limitations of the suppression algorithms or to receiver system effects causing some mismatch in the surveillance and reference signals. However, assuming this were the case, one would not expect to see such deep reduction of the zero-Doppler terms for the various algorithms, as shown in Fig. 3. In general, it is clear that regardless of the mitigation algorithm that is chosen, effective suppression values of 30–45 dB can be expected for typical PR scenarios with high INR values. Knowledge of the surveillance channel noise floor can provide a good indicator for the effective noise or interference floor of a PR system with a good reference signal quality. A carefully chosen DSI suppression algorithm can provide an effective noise figure of 6–20 dB plus the true RF noise figure.

An ideal DSI mitigation algorithm would exhibit stable suppression performance, such that the variance in suppression when analyzed over time (between multiple CPIs) was zero. Of all algorithms, the FBLMS resulted the most stable temporal performance shown in Table III across all illuminators. The other high performing algorithms (NLMS and the ECA) experienced a fair amount of CPIs where the result was unstable and suppression performance dropped significantly, the root cause of which has not yet been determined. In particular, the performance of the NLMS algorithm varied throughout the measurements of the 605-MHz illuminator shown in Fig. 10. The LS algorithm was found to be the worst for consistency and in many cases dropped to a few dB of suppression, which resulted in the very high variances for the 605- and 617-MHz illuminators shown in Table III. The behavior of the various algorithms was found to be different for each illuminator, and could not be tied to a particular physical parameter or attribute relating to the PR setup. In short, *in situ* measurements and experimental validation are necessary to maximize the effective dynamic range of a particular PR receiver.

Overall, the high levels of suppression and stable performance of the FBLMS filter, combined with its minimal runtime of all compared algorithms, resulted a very appealing candidate algorithm for DSI suppression in most PR systems with particular emphasis on real-time implementation. NLMS and the ECA algorithm did occasionally achieve better suppression values for certain CPIs, but their unstable nature would result in less predictable tracking performance, and potentially updates with varying frequency if certain CPIs are deemed unusable due to the poor performance of the mitigation algorithm. However, FBLMS is one of the fully adaptive algorithms with a clutter notch of ± 100 Hz, and therefore, for situations where slow moving targets are the primary interest, a system designer may want to choose one of the fixed coefficient algorithms, such as the ECA or LS methods to enable operation in these regions. In particular, the LS algorithm is very attractive due to its simplicity and fast runtimes, requiring no inputs for operation other than the number of filter coefficients over which to operate.

V. CONCLUSION

A comprehensive theory for the mathematical model of the PR signal model and DSI suppression was presented, along with a practical method of estimating effective

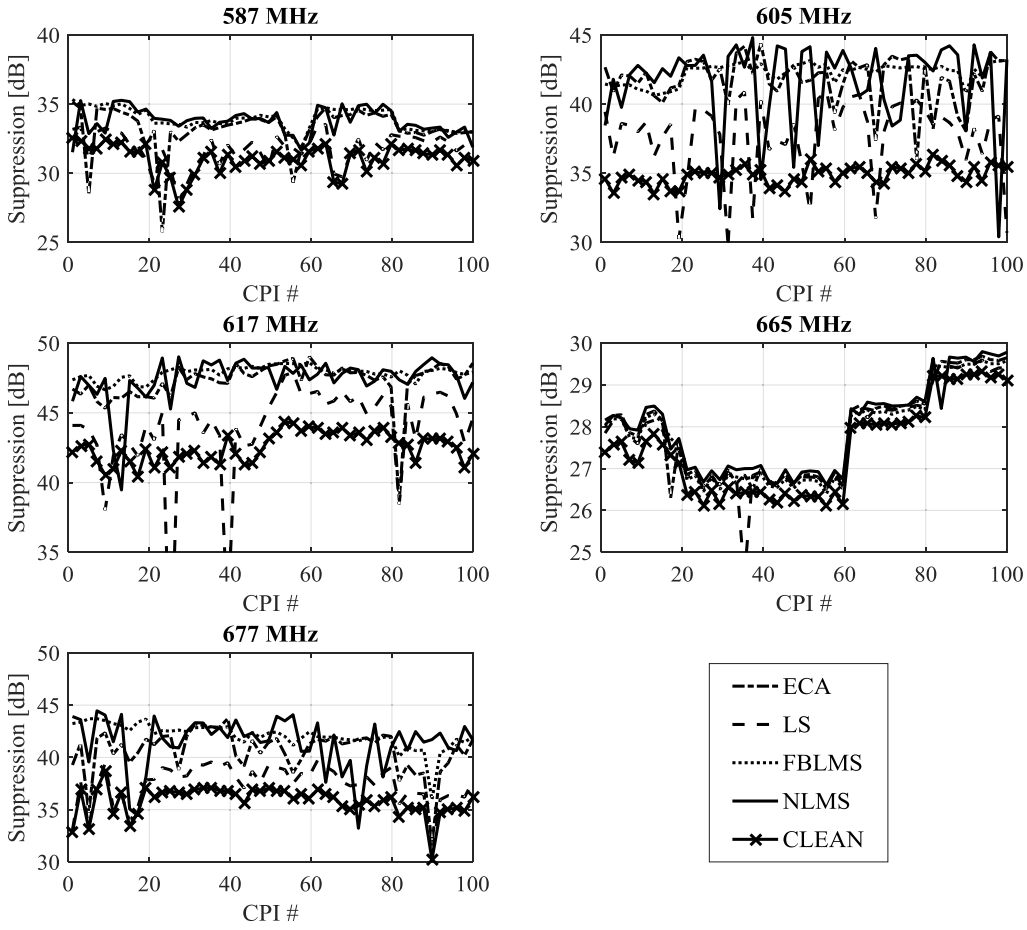

Fig. 10. DSI suppression results for 5 illuminators across 5 collections, each with 20 CPIs.

DSI suppression. Runtime, mean, and variance in suppression performance, and selection of each algorithm's tunable parameters must be evaluated and are inherently linked to the radar operational modality and objectives. The primary factors affecting suppression performance, aside from the choice of algorithm, were shown to be the physical clutter and multipath channel, purity of the reference and surveillance waveforms, as well as stationarity of the clutter coefficients throughout the CPI over which the adaptive filter is implemented. It was shown that it is often not necessary to suppress all visible clutter coefficients in the range Doppler surface to minimize the effective noise floor, as long as the sidelobes from the clutter lie below the thermal noise floor. For the experimental results shown here, this was approximately 30 km beyond the bistatic baseline for the various transmitters, which reduces the required filter taps and, therefore, computational complexity. For extended CPIs generally longer than 100 ms, it was found that the suppression performance of the fixed coefficient algorithms (ECA, LS, and CLEAN) degraded significantly due to slowly time-varying clutter coefficients, which suggest using an adaptive filter (FBLMS and NLMS). These algorithms require careful tuning of the adaptation parameters to simultaneously optimize suppression performance while maintaining a sufficiently narrow Doppler clutter null as to not blind the system to slow moving targets.

Practical implementation considerations and the configuration of many algorithms for successful operation on simulated and experimental data were given to aid the practicing engineer attempting to integrate these methods on a system. Extensive experimental results evaluating all algorithms' DSI suppression over time and frequency show that the noise floor of a PR cannot be reached in practice, and a combination of techniques (adaptive array antennas, analog suppression, reference signal remodulation, and so on) may be required to achieve this maximum dynamic range from PR systems. The effective floor after application of the DSI algorithms was shown to be approximately 6–20 dB above the thermal noise floor in the ADC, such that a large effective noise figure should be used when predicting PR performance. Results of the individual algorithms demonstrate that FBLMS and LS both represent good candidates for near real-time implementation, with runtimes under 1 s for a typical CPI of 100 ms at 10 MSa/s. The FBLMS algorithm, which has not received significant attention in the literature, was shown to be among the most favorable of all algorithms, due to the high suppression performance and minimal computational complexity and variance in suppression over time. However, the significant Doppler null width inhibits its use for slow moving target scenarios where one would benefit from LS or the ECA algorithms. Overall, DSI suppression was shown to be a

critical stage of PR processing, and selection of an algorithm is an important stage in PR system design, which requires careful consideration of a number of factors, to be aided by the discussions and results of this paper.

REFERENCES

[1] H. D. Griffiths and C. J. Baker, "Passive coherent location radar systems. Part 1: Performance prediction," *IEE Proc.-Radar, Sonar Navigat.*, vol. 152, no. 3, pp. 153–159, Jun. 2005.

[2] S. O. Haykin, *Adaptive Filter Theory*, 4th ed. Englewood Cliffs, NJ, USA: Prentice-Hall, 2001.

[3] K. Kulpa, "The CLEAN type algorithms for radar signal processing," in *Proc. Microw., Radar Remote Sens. Symp.*, Sep. 2008, pp. 152–157.

[4] F. Colone, D. W. O'Hagan, P. Lombardo, and C. J. Baker, "A multistage processing algorithm for disturbance removal and target detection in passive bistatic radar," *IEEE Trans. Aerosp. Electron. Syst.*, vol. 45, no. 2, pp. 698–722, Apr. 2009.

[5] K. S. Kulpa and Z. Czekała, "Masking effect and its removal in PCL radar," *IEE Proc.-Radar, Sonar Navigat.*, vol. 152, no. 3, pp. 174–178, Jun. 2005.

[6] M. Malanowski, "Comparison of adaptive methods for clutter removal in PCL radar," in *Proc. Int. Radar Symp.*, May 2006, pp. 1–4.

[7] J. E. Palmer and S. J. Searle, "Evaluation of adaptive filter algorithms for clutter cancellation in Passive Bistatic Radar," in *Proc. IEEE Radar Conf.*, May 2012, pp. 493–498.

[8] J. L. Garry, G. E. Smith, and C. J. Baker, "Direct signal suppression schemes for passive radar," in *Proc. Signal Process. Symp. (SPSympo)*, Jun. 2015, pp. 1–5.

[9] R. Cardinali, F. Colone, C. Ferrett, and P. Lombardo, "Comparison of clutter and multipath cancellation techniques for passive radar," in *Proc. IEEE Radar Conf.*, Apr. 2007, pp. 469–474.

[10] M. Meller and S. Tujaka, "Processing of noise radar waveforms using block least mean squares algorithm," *IEEE Trans. Aerosp. Electron. Syst.*, vol. 48, no. 1, pp. 749–761, Jan. 2012.

[11] *ATSC Digital Television Standard Part 2—RF/Transmission System Characteristics*, Adv. Television Syst. Committee, Washington, DC, USA, 2007.

[12] M. Baczyk and M. Malanowski, "Reconstruction of the reference signal in DVB-T-based passive radar," *Int. J. Electron. Telecommun.*, vol. 57, no. 1, pp. 43–48, 2011.

[13] W. C. Barott and J. Engle, "Single-antenna ATSC passive radar observations with remodulation and keystone formatting," in *Proc. IEEE Radar Conf.*, May 2014, pp. 159–163.

[14] S. Searle, S. Howard, and J. Palmer, "Remodulation of DVB–T signals for use in Passive Bistatic Radar," in *Proc. Conf. Rec.-Asilomar Conf. Signals, Syst. Comput.*, Nov. 2010, pp. 1112–1116.

[15] N. J. Willis, *Bistatic Radar*. Rayleigh, U.K.: SciTech, 1995.

[16] N. J. Willis and H. D. Griffiths, *Advances in Bistatic Radar*, 1st ed. Rayleigh, U.K.: SciTech Publishing, 2007.

[17] S. J. Searle, J. E. Palmer, H. A. Harms, and L. M. Davis, "Impact of quantization on passive radar target detection," in *Proc. IET Int. Conf. Radar Syst. (Radar)*, Oct. 2012, p. 44.

[18] J. L. Garry, G. E. Smith, and C. J. Baker, "Wideband DTV passive ISAR system design," in *Proc. IEEE Radar Conf. (RadarCon)*, May 2015, pp. 834–839.

[19] J. B-Y. Tsui, *Digital Techniques for Wideband Receivers*, 2nd ed. Rayleigh, U.K.: SciTech Publishing, 2004.

[20] R. Cardinali, F. Colone, P. Lombardo, O. Crognale, A. Cosmi, and A. Lauri, "Multipath cancellation on reference antenna for passive radar which exploits FM transmission," in *Proc. IET Int. Conf. Radar Syst.*, Oct. 2007, pp. 1–5.

[21] M. Meller, "Cheap cancellation of strong echoes for digital passive and noise radars," *IEEE Trans. Signal Process.*, vol. 60, no. 5, pp. 2654–2659, May 2012.

[22] M. Malanowski, K. Kulpa, and K. E. Olsen, "Extending the integration time in DVB-T-based passive radar," in *Proc. Eur. Radar Conf. (EuRAD)*, Oct. 2011, pp. 190–193.

[23] K. Chetty, G. E. Smith, and K. Woodbridge, "Through-the-wall sensing of personnel using passive bistatic WiFi radar at standoff distances," *IEEE Trans. Geosci. Remote Sens.*, vol. 50, no. 4, pp. 1218–1226, Apr. 2012.

[24] X. Guan, D.-H. Hu, L.-H. Zhong, and C.-B. Ding, "Strong echo cancellation based on adaptive block notch filter in passive radar," *IEEE Geosci. Remote Sens. Lett.*, vol. 12, no. 2, pp. 339–343, Feb. 2015.

[25] Y. Feng, T. Shan, S. Liu, and R. Tao, "Interference suppression using joint spatio-temporal domain filtering in passive radar," in *Proc. IEEE Radar Conf. (RadarCon)*, vol. 3. May 2015, pp. 1156–1160.

Joseph Landon Garry (M'08) was with the Air Force Research Laboratory (AFRL), OH, USA, investigating a number of various radar applications, until 2014. He is currently a Research Associate with The Ohio State University, Columbus, OH, USA, where he is helping lead the direction for passive radar research with the Cognitive Sensing Group, ElectroScience Laboratory. His research interests include synthetic aperture radar and Inverse SAR imaging, passive radar systems and algorithm development, MIMO radar, fully adaptive radar, and automotive radar.

Chris J. Baker (SM'06–F'16) was an Ohio State Research Scholar in integrated sensor systems with The Ohio State University, Columbus, OH, USA. Until 2011, he was the Dean and the Director with the College of Engineering and Computer Science, Australian National University, Canberra, Australia. He held the Thales-Royal Academy of Engineering Chair of Intelligent Radar Systems at University College London, London, U.K. He has been involved in radar systems research since 1984. He is currently the Chief Technology Officer with Aveillant, Cambridge, U.K., with responsibilities for all technical aspects of the company's products and their development. He is also a Visiting Professor with the University of Cape Town, Cape Town, South Africa, Wright State University, Dayton, OH, USA, Strathclyde University, Glasgow, U.K., and Birmingham University, Birmingham, U.K. He has authored over two hundred and fifty publications on a range of issues including *Coherent Radar Techniques*, *Radar Signal Processing*, *Radar Signal Interpretation*, *Electronically Scanned Radar Systems*, *Radar Imaging*, and *Natural and Cognitive Echo Locating Systems*.

Dr. Baker is a Fellow of the IET. He was a recipient of the IEE Mountbatten Premium (twice) and the IEE Institute Premium.

Graeme E. Smith (M'07–SM'11) was with Villanova University, Villanova, PA, USA. He held post-doctoral positions at University College London, London, U.K. Between 1999 and 2004, he was a Lead Systems Engineer with BAE SYSTEMS, Luton, UK developing radar warning receivers. He is currently a Research Assistant Professor with The Ohio State University, Columbus, OH, USA, where he leads the Cognitive Sensing Group and teaches an introductory course on radar systems. He is also a Visiting Professor with University College London. He has authored five book chapters and over eighty journal and conference papers. His research interests include, cognitive/fully adaptive radar processing, flow fields for echolocation, passive radar, multistatic radar clutter, radar target recognition/classification, micro-Doppler signatures, and through-the-wall radar imaging.

Dr. Smith is a member of the IET.